

RSC Advances



This is an *Accepted Manuscript*, which has been through the Royal Society of Chemistry peer review process and has been accepted for publication.

Accepted Manuscripts are published online shortly after acceptance, before technical editing, formatting and proof reading. Using this free service, authors can make their results available to the community, in citable form, before we publish the edited article. This *Accepted Manuscript* will be replaced by the edited, formatted and paginated article as soon as this is available.

You can find more information about *Accepted Manuscripts* in the [Information for Authors](#).

Please note that technical editing may introduce minor changes to the text and/or graphics, which may alter content. The journal's standard [Terms & Conditions](#) and the [Ethical guidelines](#) still apply. In no event shall the Royal Society of Chemistry be held responsible for any errors or omissions in this *Accepted Manuscript* or any consequences arising from the use of any information it contains.

Calcination system-induced nanocasting synthesis of uniform Co_3O_4 nanoparticles with high surface area and enhanced catalytic performance

Xiaohong Sun,^{*,†} Rui You,[‡] Xudong Hu,[†] Junbin Mo,[†] Rui Xiong,[†]
Huiming Ji,[†] Xiaolei Li,[†] Shu Cai,[†] Chunming Zheng^{*,§} and Ming
Meng[‡]

ABSTRACT: Co_3O_4 catalytic materials with various mesoporous periodicity and crystallinity have been successfully synthesized via a calcination system-induced nanocasting method. N- Co_3O_4 with uniform nanoscale morphology, high specific surface area, and large pore size distribution was obtained in open system as calcination process, while M- Co_3O_4 with long-range mesoporous periodicity and high crystallinity was synthesized using close system as the calcination condition. The control of the mesostructure and morphology was carried out by tuning the diffusion rate of cobalt precursor in template channel resulting from the different escape rate of the decomposed byproducts via the varied calcination containers. The CO oxidation testing indicated N- Co_3O_4 exhibited better catalytic performance than that of M- Co_3O_4 . The difference in activity could be attributed to the uniform nanoscale structure of N- Co_3O_4 , which mesoporous M- Co_3O_4 lacked. N- Co_3O_4 had the better performance of CO oxidation due to the uniform nanoparticles structure, higher specific surface area, larger pore size distribution, abundant active oxygen species and Co^{3+} cationic species on the surface, which accelerated the adsorption and diffusion of reactant molecules and finally improve the reaction activity of N- Co_3O_4 . The resulting catalytic behaviors lead to a better understanding of designing and using such metal oxides for a number of catalytic applications.

[†]School of Materials Science and Engineering, Key Lab of Advanced Ceramics and Machining Technology, Tianjin University, Tianjin 300072, PR China. E-mail: sunxh@tju.edu.cn

[‡]School of Chemical Engineering and Technology, Tianjin University, Tianjin 300072, PR China.

[§]State Key Laboratory of Hollow-fiber Membrane Materials and Membrane Processes, School of Environmental and Chemical Engineering, Tianjin Polytechnic University, Tianjin 300387, PR China. E-mail: zhengchunming@tjpu.edu.cn

Introduction

Heterogeneous catalysis has attracted much attention over the past decades due to its paramount importance in many areas of the chemical and energy industries.¹⁻⁴ In general, for heterogeneous catalysis, the reactants diffuse to the catalyst surface and adsorb onto it, via the formation of chemical bonds.^{5,6} After catalytic reaction, the products desorb from the catalyst surface and diffuse away.⁷⁻⁹ Hence, based on the transport phenomena and surface chemistry, the improvement of diffusion and adsorption of reactant molecules would be very important for promoting the catalytic performance.¹⁰⁻¹²

Nanostructure metal oxide materials (such as Co_3O_4 ,¹³ CuO ,¹⁰ NiO ,¹⁴ Mn_3O_4 ,¹⁵ TiO_2 ,¹⁶ and CeO_2 ¹⁷) with low cost and high thermal stability have been well studied and developed in the past decade because their large specific surface and high surface-to-volume ratio will provide more reactants diffusion and catalytic sites, which can obtain the improved catalytic activity.^{9,11,18} In order to get the larger reaction surface areas and more active sites, synthesis of catalytic materials with small particle size is the common approach.¹⁹⁻²² Surfactants are widely used to control the materials size during the synthesis of nanoscale catalysts.^{23,24} Generally, the used surfactants are easily removed by washing or calcination at higher temperatures, while some others are very stubborn.²⁵ Especially, when the materials size comes smaller, their surface energy turns to be much larger, which will lead to the stronger adsorption of surfactants on the catalysts surface and make them contaminated and passivate in the catalysis application.^{26,27} Narayana et al. found that the addition of biphenyl and PVP to

the nanoparticles catalysts preparation process results in the poisoning the active sites and the decreasing the catalytic efficiency due to capping of the catalysts surface.²⁸ If heating process is used to thoroughly remove the surfactants adsorbed on the catalysts surface, due to the small nanoscale size and high surface energy, particle aggregation and crystals growth will not be avoided.²⁵ As a result, the surface areas, active sites, and catalytic activity are decreased at the same time. Hence, the synthesis of nanocatalysts with high surface area, enough reaction sites, and clean active surface is an important concern.

Among the preparation methods for metal oxide nanocatalysts, the nanocasting method (hard template) has recently attracted great interest.²⁹⁻³¹ It involves the synthesis of a mesoporous template (such as hexagonal SBA-15, cubic KIT-6, or ordered mesoporous carbon), the conversion of metal precursor to metal oxide inside the channel of template by calcination, and the etching of hard template leaving the guest replica with the template topological structure.^{32,33} Enhanced catalytic features can be expected for the metal oxides prepared through this method, because hard templates can provide stable supports for high-temperature crystallization, that results the nanocrystalline and mesoporous catalysts with high surface area, large diffusion channel, and clean active sites.³⁴ Lots of mesoporous metal oxides (Fe_2O_3 , Cr_2O_3 , In_2O_3 , CeO_2 , Co_3O_4 , NiO , MoO_2 and Mn_3O_4) have been successfully prepared by nanocasting method.³⁵⁻³⁷ Recently, we reported a universal and effective calcination container effect in the nanocasting synthesis of mesoporous metal oxides, by which, the mesostructured periodicity, as well as particle size, porous size distribution, and specific surface area of the nanocasted metal oxide replicas can be controlled in a large range.³⁸ It is well known that the microstructure and morphology of metal oxide catalysts

plays an important role in their catalytic performance.¹⁵ To the best of our knowledge, the mesostructured periodicity effect of nanocasted metal oxide catalysts with respect to their catalytic performance are seldom considered and investigated because of the difficulty in controlling the mesostructured periodicity and related structure and morphology parameters.

In this work, to extend the nanocasting synthesis of metal oxides with various morphology and structure and to deepen the comprehension of calcination system-induced control behaviors for their related applications, Co_3O_4 acts as a model material to study the CO oxidation properties based on its different nanostructures. Close system and open system are respectively used to control the diffusion of cobalt precursor during the nanocasting calcination process and finally get the mesoporous M- Co_3O_4 with long-range mesoporous periodicity and uniform N- Co_3O_4 nanoparticles with high specific surface area. The catalytic performance of both Co_3O_4 samples for CO oxidation was systematically investigated and the results indicated that N- Co_3O_4 exhibited better catalytic activity compared with that of M- Co_3O_4 . A possible enhancement catalytic mechanism of N- Co_3O_4 was proposed based on its structure, morphology and CO oxidation property.

Experimental

Synthesis

All chemical reagents are of analytical grade and used without further purification. Ordered mesoporous silica template KIT-6 with *Ia3d* symmetry was firstly synthesized following the previous reports of Ryoo's group.³⁹ Mesoporous Co_3O_4 samples with different mesoporous

periodicity morphology and structure, including specific surface area, porous size distribution, and crystallinity, were synthesized according to our previous reported general nanocasting way to prepare ordered mesoporous metal oxides with controlled mesostructure in a large range.³⁸ To prepare uniform nanoscale Co_3O_4 with short-range mesoporous periodicity (named N- Co_3O_4), an improved “open system” nanocasting method was adapted as described below. Typically, 4.9 g of KIT-6 silica template was mixed with 100 mL of toluene and heated to 65 °C. Then 9.8 g of cobalt nitrate hexahydrate ($\text{Co}(\text{NO}_3)_2 \cdot 6\text{H}_2\text{O}$) was added into the mixture and kept in continuous mechanical stirring for 5 h. Since the melting point of $\text{Co}(\text{NO}_3)_2 \cdot 6\text{H}_2\text{O}$ is less than 65 °C, under heating and stirring, it will melt and liquefy, and automatically move into the KIT-6 template pores due to the capillary condensation interaction between nitrate and silica inner pore surface. The cobalt precursor@silica composites were obtained by evaporation of solvent in air at 40 °C overnight. The annealing or calcination process in air was the crucial step to prepare the Co_3O_4 with totally different morphology and structure. The “open system” nanocasting way to obtain the N- Co_3O_4 @KIT-6 and N- Co_3O_4 was conducted by calcining the precursor@silica composites in a muffle furnace using Petri dish (diameter of 60 mm and depth of 12 mm) as the sample container with a heating rate of 2 °C min^{-1} from room temperature to 450 °C and kept at that temperature for 5 h. After calcination, the obtained N- Co_3O_4 @silica samples were treated with 2 M NaOH solution twice to remove the silica template, and then centrifuged, washed with water and ethanol for several times and air-dried at 60 °C to finally get the N- Co_3O_4 . In contrast, highly ordered mesoporous Co_3O_4 with long-range mesoporous periodicity (named M- Co_3O_4) was synthesized using the similar nanocasting method as N- Co_3O_4 but the

different calcination container (called “close system”). This process was performed using glass bottle (diameter of 12 mm and depth of 45 mm) with a glass strip for 100 % coverage as the thermal-treatment container for the calcination of as-obtained cobalt precursor@silica composites. The calcination temperature program was totally same with that for N-Co₃O₄. Sum up, in order to avoid the other synthesis parameters effect, two sets of samples were prepared from the same batch and subjected to the same calcination temperature procedure but different calcination containers (called calcination systems): M-Co₃O₄ was synthesized by loading the cobalt precursor@KIT-6 intermediate in a glass bottle with a glass strip for 100 % coverage (close system), while N-Co₃O₄ was prepared by spreading the intermediate in a Petri dish without any cover (open system). Such differences in the container conditions during calcination are sufficient to change the morphology and structure of the Co₃O₄ samples and have a profound influence on their CO oxidation behavior, as demonstrated later.

Characterization

The wide-angle X-ray powder diffraction (XRD) patterns of the dry samples were performed at room temperature on a Philips X'pert powder Diffractometer with a graphite monochromator and Fe K α 1 source ($\lambda = 0.193$ nm). Typically, the data were collected from 10° to 90° with a resolution of 0.2°. The average crystallite size was estimated from the Debye-Scherrer equation, $D = K\lambda/(\beta \cos \theta)$, where D is the average crystal diameter, β is the corrected peak width (full width at half-maximum), K is a constant related the shape of the crystallites (K = 0.94), λ is the wavelength of the X-rays employed, and θ is the diffraction angle. The width of the diffraction peak with the highest intensity was selected for the calculation. The small-angle X-ray diffraction (SAXRD) data were taken on a Philips X'pert

MPD thin film powder XRD using an Cu K α radiation ($\lambda = 0.154$ nm). Transmission electron microscopy (TEM) measurements were performed on a FEI Tecnai G2 F20 microscope. All samples subjected to TEM measurements were ultrasonically dispersed in alcohol and drop-cast onto copper grids. The SEM images were measured on a FEI XL40 instrument. Nitrogen adsorption and desorption isotherms were measured at 77 K on a Micromeritics TriStar porosimeter apparatus. The samples were outgassed at 150 °C overnight before measurements were made. The surface area was obtained by the Brunauer-Emmett-Teller (BET) method and the pore size distribution was calculated from the adsorption branch of the isotherm using the Barrett-Joyner-Halanda (BJH) method. Surface elemental analysis was performed using an ESCALAB250 X-ray photoelectron spectroscopy (XPS). Temperature-programmed reduction (H₂-TPR) measurements were performed on a Thermo-Finnigan TPDRO 1100 instrument equipped with a thermal conductivity detector (TCD). 10 mg of powder sample were heated from room temperature to 900 °C at a rate of 10 °C/min with a gaseous mixture of 5 vol. % H₂/N₂ at a flow rate of 20 ml/min. Before detection, the gas was purified by a solid trap containing CaO and NaOH materials in order to remove the H₂O and CO₂.

Catalytic performance measurements

Oxidation of CO was carried out in a continuous flow fixed-bed quartz tubular reactor (i.d. 8 mm) mounted in a tube furnace. The weight of catalyst was 0.2 g. The reaction gas consisting of 1% CO, 20% O₂ and balance N₂ was fed at a rate of 30 mL min⁻¹. Reaction temperature was measured by a thermo-couple in the middle of catalyst bed. The feed and product mixtures were analyzed by a gas chromatograph (Agilent 7890A) equipped with a thermal

conductivity detector. The CO conversion X : $X = (\text{CO}_{\text{in}} - \text{CO}_{\text{out}}) / \text{CO}_{\text{in}}$.

Results and discussion

The controlled synthesis of Co_3O_4 using nanocasting method with different calcination systems was characterized by the wide-angle X-ray powder diffraction (XRD). As shown in Fig. 1a, after the KIT-6 template is etched, well-defined diffraction peaks indicate the crystalline nature and all of the peaks correspond well to the face-centered cubic spinel phase of Co_3O_4 (JCPDS card No. 42-1467).^{25,40,41} No characteristic other peaks were observed, indicating the presence of pure Co_3O_4 . The XRD peaks width of N- Co_3O_4 calcined in open system is larger than that of M- Co_3O_4 synthesized in close system, which suggests the smaller crystallite size of N- Co_3O_4 than that of M- Co_3O_4 . Based on the Debye-Scherrer equation for the full-width at half-maximum (fwhm) of the (311) reflection, the average crystallite sizes of N- Co_3O_4 and M- Co_3O_4 are calculated to be 9.5 and 12.6 nm, respectively, which indicates that the crystallinity and crystallite size of Co_3O_4 can be controlled by the varied calcination systems for nanocasting method. From the XRD patterns of Co_3O_4 @KIT-6 samples without the template removing, one can see a weak broadening band, corresponding to the presence of amorphous silica template. Small-angle X-ray diffraction (SAXRD, shown in Fig. 1b) was carried out to prove the difference in mesoporous periodicity of as-synthesized Co_3O_4 by different calcination systems. SAXRD diffraction pattern of KIT-6 corresponds to the 211 and 220 diffraction peaks, revealing that the KIT-6 template consists uniquely of large ordered mesoporous domains of pure bicontinuous mesostructure with

cubic $Ia3d$ symmetry.³⁹ The SAXRD pattern of $M\text{-Co}_3\text{O}_4$ shows one intense peak at 2θ of around 0.93° , corresponding to the 211 diffraction peak of $Ia3d$ symmetry, which indicates that the long-range mesoporous periodicity of KIT-6 is well retained in $M\text{-Co}_3\text{O}_4$. The 211 peak of $M\text{-Co}_3\text{O}_4$ shifting to the larger degree compared with that of KIT-6 can be attributed to the smaller mesoporous size of $M\text{-Co}_3\text{O}_4$ than that of silica template, which will be proved by the following N_2 physisorption analysis. Comparing to the SAXRD pattern of $M\text{-Co}_3\text{O}_4$, the broadening 211 peak of $N\text{-Co}_3\text{O}_4$ with weak intensity indicates that there is a reduction in the X-ray scattering contrast between the pore and the framework and the mesoporous periodicity of $N\text{-Co}_3\text{O}_4$ is much lower than that of $M\text{-Co}_3\text{O}_4$.³³

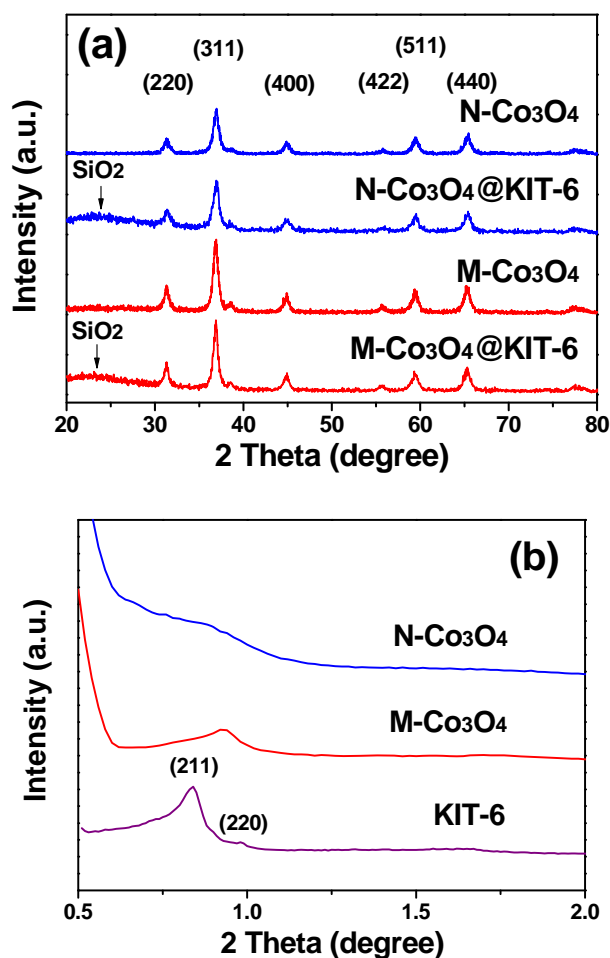


Fig. 1 XRD patterns (a) of $M\text{-Co}_3\text{O}_4@KIT\text{-6}$, $M\text{-Co}_3\text{O}_4$, $N\text{-Co}_3\text{O}_4@KIT\text{-6}$, and $N\text{-Co}_3\text{O}_4$; SAXRD patterns (b) of KIT-6, $M\text{-Co}_3\text{O}_4$, and $N\text{-Co}_3\text{O}_4$.

The mesoporous periodicity and morphology control of as-synthesized Co_3O_4 with changed calcination systems can also be confirmed by the TEM and SEM characterization. The TEM image shown in Fig. 2a reveals that M- Co_3O_4 samples are with highly ordered mesostructure. In contrast, from Fig. 2b for N- Co_3O_4 , one can see the presence of uniform isolated nanoparticles with diameter ca. 10 nm and without long-range mesoporous periodicity, which is in good agreement with the above SAXRD data. Since the calculated average crystallite size of N- Co_3O_4 using Debye-Scherrer equation is 9.5 nm, which is almost equal to the observed TEM particle size of N- Co_3O_4 , indicating that each nanoscale particle of N- Co_3O_4 is consisted of single crystalline. In this work, owing to the synthesis of Co_3O_4 using the nanocasting “hard-template” method without adding of surfactant, KIT-6 template will supply the hard-supporting during the calcination process for the conversion of cobalt precursor to Co_3O_4 . Hence, for “open system” synthesis, uniform and dispersed nanoscale N- Co_3O_4 single crystalline with clean surfaces can be obtained. The nanocasting synthesized nanoscale Co_3O_4 particles will not aggregate easily compared to the traditional synthesized nanoparticles and are supported to have high catalytic activity. The SEM images of both Co_3O_4 samples are shown in Fig. 2c and d. M- Co_3O_4 and N- Co_3O_4 exhibit nearly spherical particles. Their morphology is totally different from their parent template KIT-6, which is irregular in shape and much larger than the replica.³⁹ M- Co_3O_4 samples are with long-range mesoporous periodicity and wide particle size distribution from ca. 1 μm to ca. 10 μm . In contrast, N- Co_3O_4 samples are consisted of uniform nanoscale particles with particle size of ca. 10 nm. Obviously, the mesoporous periodicity and particle sizes of the Co_3O_4 samples can be controlled easily using the improved nanocasting method with changed calcination systems.

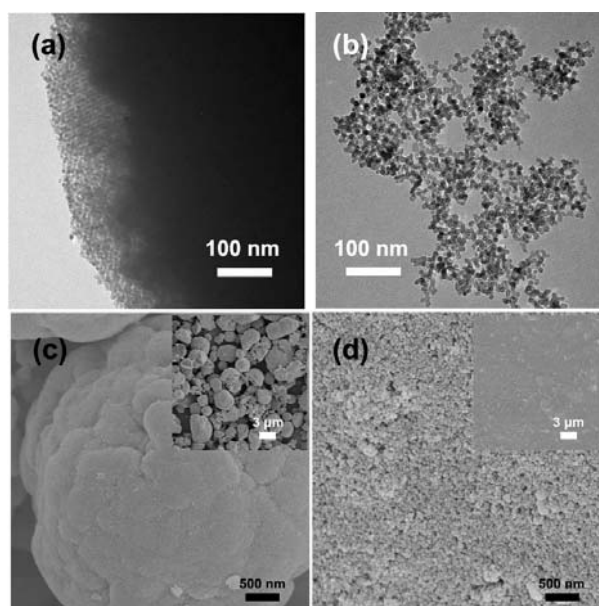


Fig. 2 TEM images of M-Co₃O₄ (a) and N-Co₃O₄ (b); SEM images with low resolution (inset) and high resolution of M-Co₃O₄ (c) and N-Co₃O₄ (d).

The N₂ physisorption isotherms and pore size distributions data of both Co₃O₄ replica samples are shown in Fig. 3. The Brunauer-Emmett-Teller (BET) specific surface area and pore volume of N-Co₃O₄ are 130.2 m² g⁻¹ and 0.4664 cm³ g⁻¹, respectively, much larger than that of M-Co₃O₄ (104.7 m² g⁻¹ and 0.1518 cm³ g⁻¹) and most reported hard-templated Co₃O₄ replicas (82-95 m² g⁻¹ and 0.14-0.18 cm³ g⁻¹).⁴²⁻⁴⁵ Both Co₃O₄ samples exhibit a typical IV isotherm with a H1-type hysteresis loop, which is characteristic for mesoporous materials.³³ The capillary condensation of N-Co₃O₄ occurs at a higher relative pressure ($P/P_0 \sim 0.90$) than that of M-Co₃O₄, indicating much larger mesoporous diameters, a fact also substantiated by the pore size distributions calculated by the Barrett-Joyner-Halenda (BJH) method using the adsorption branch of the nitrogen adsorption isotherm (Fig. 3b).³² The pore size distribution of N-Co₃O₄ is in a large range from ca. 6.0 nm to ca. 39 nm, which arises from the piled porosity by the aggregation of Co₃O₄ nanoparticles. In contrast, for M-Co₃O₄, two steps of capillary condensation corresponding to two pore size distributions (1.9 nm and 5.7 nm) can be observed. The former pore is caused by the replica from the KIT-6 template, and a narrow

pore size distribution confirms the ordered uniform pore structure. The latter piled porosity with large pore size distribution comes from the aggregation of mesoporous particles, which confirms the observation from the SEM image.³³ All the above data indicate that the different calcination system nanocasting method have a significant effect on the mesoporous periodicity, pore size distribution, crystallinity, and particle size of the as-synthesized Co_3O_4 samples. This improved method makes it possible to research the relationship between the mesoporous structure and morphology of Co_3O_4 and their corresponding catalytic properties, which to the best of our knowledge has never been researched.

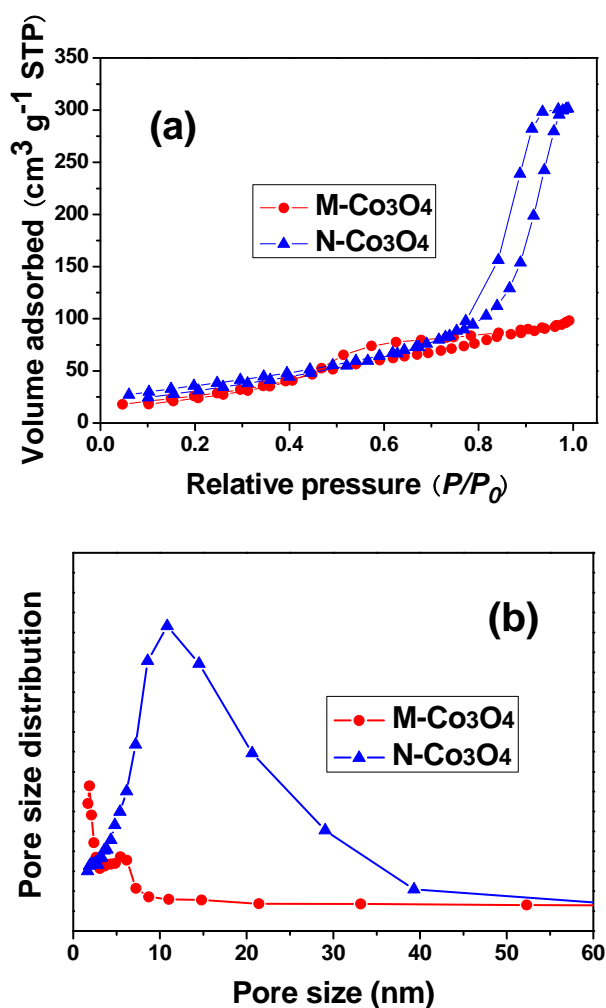


Fig. 3 Nitrogen physisorption isotherms (a) and pore size distributions (b) of M-Co₃O₄ and N-Co₃O₄.

Fig. 4 schematically illustrates the calcination system effect mechanism of Co_3O_4 synthesized using the improved nanocasting method. In this work, in order to avoid the other synthesis parameters effect, two sets of samples were prepared from the same batch and subjected to the same calcination procedure but different calcination containers (close system and open system). Highly ordered mesoporous M- Co_3O_4 with large particle sizes are obtained when they are calcined in close system. In contrast, uniform nanoscale N- Co_3O_4 synthesized in open system give small nanoparticles with high surface area. The effect mechanism can be ascribed to the container (calcination systems) influence on the escape rate of water and nitrogen oxide byproducts decomposed from the cobalt nitrate hexahydrate precursor, which in turn affects the diffusion rates of cobalt precursor during calcination and the structure and morphology of final Co_3O_4 products (Fig. 4). During calcination, the entire container is saturated with water vapor, which comes from the cobalt precursor solution and reduces of the water content of the cobalt precursor@silica. Hence, the container opening can be utilized to tune the residual water amount within the inner pore space of the KIT-6 template, and thus be used to control the transportation rate of the cobalt precursor in KIT-6. When the calcination container is close system, the fast evaporation of water vapor from the system is hard to be achieved, which keeps the decomposition of cobalt precursor in a liquid form, promote the diffusion of cobalt precursor and finally obtains the Co_3O_4 sample with large particle size, as well as corresponding large mesoporous periodicity and high crystallinity. For open system nanocasting synthesis, water is rapidly evaporated up to the open space when the calcination temperature is higher than the melting of cobalt nitrate hexahydrate, which causes solidification of the precursors before their decomposition. The solid-to-solid

conversion inhibits the long-distance transportation of the cobalt species and thus isolated nanoparticles with uniform size are formed inside the mesopore channels. In short, different calcination systems for nanocasting synthesis can be easily utilized to control the mesoporous periodicity of as-synthesized Co_3O_4 , as well as the crystallinity, porous size distribution, specific surface area, and particle size.³⁸ Furthermore, in nanocasting synthesis of metal oxides, metal nitrates are the most commonly used metal precursors because they can be readily impregnated into the mesoporous templates and then in situ converted to corresponding metal oxides. During the calcination conversion, distinct volume shrinkage occurs due to the weight loss and density increase. Theoretical estimations based on the chemical reaction equations and bulk density data reported in our previous work reveal that only 8.54% of the pore space is occupied by Co_3O_4 after the calcination conversion when the mesoporous template is 100% filled with cobalt nitrates at the beginning.³⁸ That means the proportions between cobalt nitrate and KIT-6 silica template do not affect the final obtained mesoporous structure of Co_3O_4 a lot. It is because when the KIT-6 is excessive, only part of the mesopore spaces of KIT-6 will be used as the template. Then the calcination container system and corresponding metal precursor transportation rate will be the crucial factor to affect the pore structure of as-obtained Co_3O_4 , which has been proved above. When the cobalt nitrate is excessive compared to the KIT-6 template, the excessive cobalt nitrate will convert to Co_3O_4 outside of the mesoporous template, resulting the presence of partial imporous Co_3O_4 . Hence, in nanocasting synthesis of mesoporous metal oxides, in order to get the metal oxides with uniform mesopore structure, the proportions between cobalt nitrate and KIT-6 silica template must be controlled below 100% filling of cobalt nitrates to template

spaces.

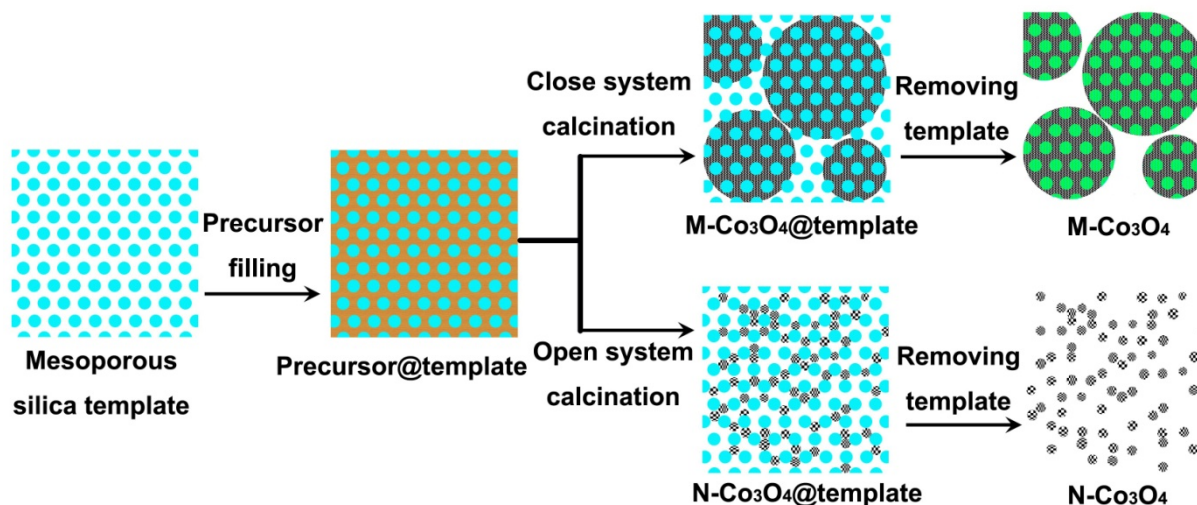


Fig. 4 Calcination system effect mechanism of Co_3O_4 synthesized using nanocasting method.

In this work, CO oxidation as a typical probe reaction for Co_3O_4 catalytic materials was carried out to test their catalytic properties. The morphology and structure influence of Co_3O_4 replicas synthesized using the different calcination systems on their corresponding catalytic performance are shown in Fig. 5a. The as-synthesized N- Co_3O_4 samples with uniform nanoscale morphology exhibit excellent CO oxidation catalytic activity. The values of T50 (the light-off temperature and the temperature for 50% conversion) of the CO for N- Co_3O_4 is ca. 88 °C. At 121 °C, the CO conversion rate becomes 100%. The T50 and 100% CO conversion temperature of M- Co_3O_4 with long-range mesoporous periodicity are ca. 100 and 131 °C, respectively, which are both higher than that of N- Co_3O_4 . It means that N- Co_3O_4 replicas exhibit higher catalytic activity than that of M- Co_3O_4 and “open system” nanocasting method is an effective way to synthesize high active nanoscale Co_3O_4 catalytic materials. To further study the influence of mesoporous morphology and surface structure, we have also tested the catalytic properties of Co_3O_4 @KIT-6 intermediate samples obtained by calcination

of cobalt precursor@KIT-6 in different calcination systems (see Fig. 5b). From the result it could be seen that N-Co₃O₄@KIT-6 and M-Co₃O₄@KIT-6 exhibit the similar CO oxidation activity with the same 100 % CO conversion temperature of 190 °C, much higher than that of N-Co₃O₄ (121 °C) and M-Co₃O₄ (131 °C), which means that Co₃O₄@KIT-6 exhibit a lower activity than the corresponding Co₃O₄ replicas after the silica template was etched. Metal oxide catalysts are often loaded on supports with porous structure and high surface area to maintain a high dispersion of the active components and to get the high catalytic activity.¹⁵ Porous silica supports are often reported to promote the activity of loaded catalysts because of the stabilization of active species in the porous structure.⁴³ However, in this work, both Co₃O₄@KIT-6 samples with different Co₃O₄ crystalline structure and morphology have the similar CO conversion properties but much lower than that of the Co₃O₄ replicas without the support templates, which has also been observed in other nanocasted Co₃O₄ catalysts for CO oxidation.^{46,47} Furthermore, the CO oxidation activity of N-Co₃O₄ replica is much better than that of M-Co₃O₄ replica after the etching of KIT-6, which means that in this work KIT-6 template does not act as the supposed support to promote the catalytic activity but acts as the catalytic surface inhibiting coating and limit the exposure of more clean reaction surface and active sites of Co₃O₄.

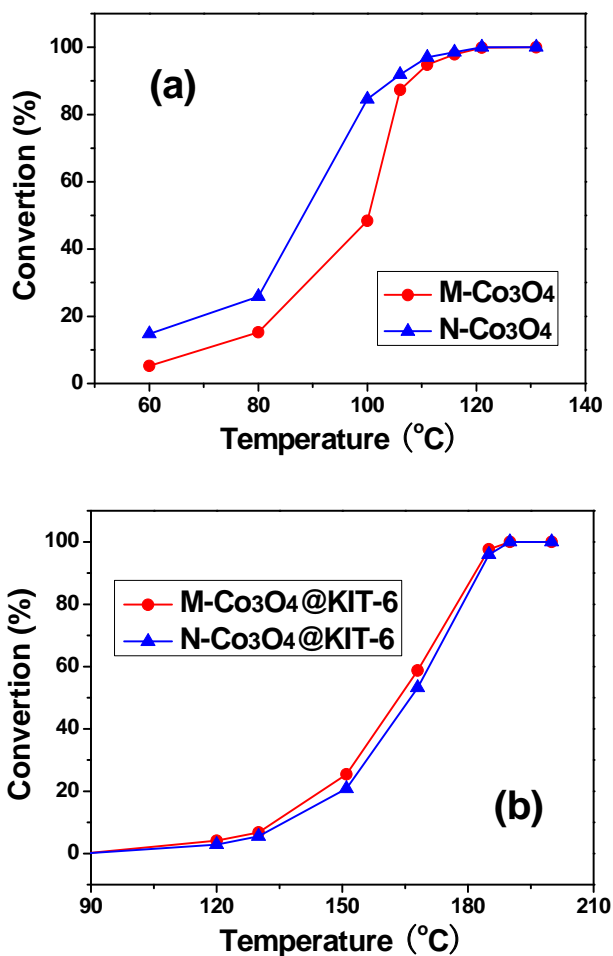


Fig. 5 Conversion as a function of temperature for CO oxidation over M-Co₃O₄ and N-Co₃O₄ (a) and M-Co₃O₄@KIT-6 and N-Co₃O₄@KIT-6 (b).

The above analysis can also be supported by the N₂ physisorption isotherms and pore size distributions data of Co₃O₄ samples before and after the removing of the KIT-6 template (see Fig. 3 and Fig. 6). The BET specific surface area of N-Co₃O₄@KIT-6 and M-Co₃O₄@KIT-6 are as high as 427.2 and 372.2 m² g⁻¹, respectively, much higher than that of N-Co₃O₄ (130.2 m² g⁻¹) and M-Co₃O₄ (104.7 m² g⁻¹). However, most of the surface area of Co₃O₄@KIT-6 samples comes from the mesoporous structure of template KIT-6, which is not active for catalytic reaction. At the same time, the active surface of Co₃O₄ loaded in KIT-6 could not be completely exposed for the tight contact of Co₃O₄ and the silica template within the mesoporous channels, which could be proved by the decreased BET specific surface area,

pore volume and pore size distributions of $\text{Co}_3\text{O}_4@\text{KIT-6}$ samples compared with KIT-6 (see Fig. 6). Hence, synthesis of Co_3O_4 replicas using the improved nanocasting method by changing the calcination systems is a better way to obtain the high activity catalytic materials with more clean and active surface areas. “Open system” calcination induced N- Co_3O_4 replicas with uniform nanoparticle size and higher specific surface area are proved to exhibit the enhanced CO oxidation catalytic properties.

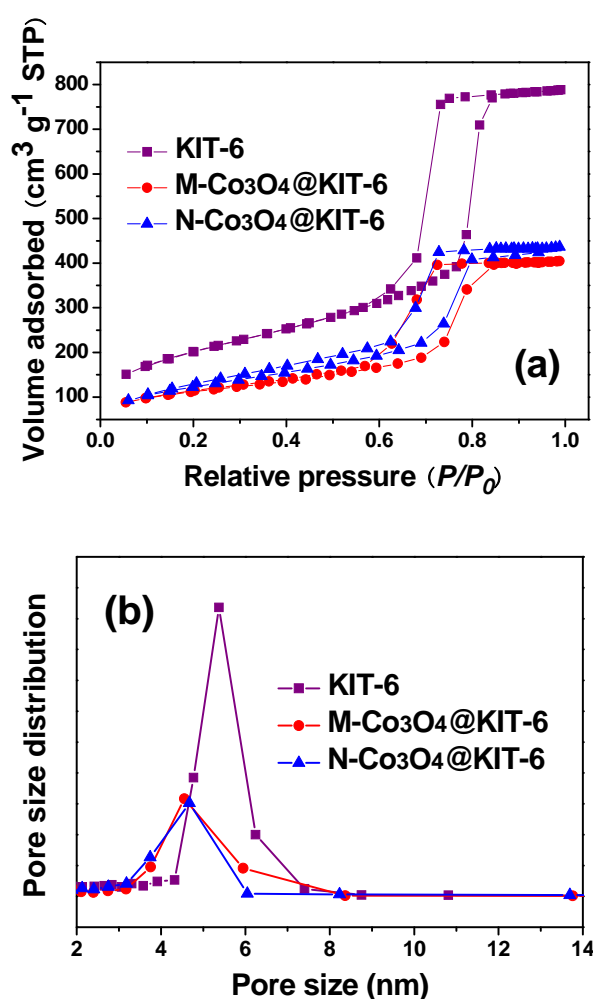


Fig. 6 Nitrogen physisorption isotherms (a) and pore size distributions (b) of KIT-6, $\text{M-Co}_3\text{O}_4@\text{KIT-6}$, and $\text{N-Co}_3\text{O}_4@\text{KIT-6}$.

In order to understand the correlation between the reducibility features of the as-synthesized Co_3O_4 replicas and their catalytic performance, the H_2

temperature-programmed reduction (H_2 -TPR) measurements of N- Co_3O_4 and M- Co_3O_4 samples were carried out and shown in Fig. 7. Three typical reduction peaks were observed for both Co_3O_4 samples, which correspond to the reduction of surface oxygen species at ca. 180 °C (α_1), the reduction of Co_3O_4 to CoO characterized by a relatively well-defined peak centered at ca. 280 °C (α_2), and the reduction of CoO to metallic cobalt with a broad high-temperature peak associated with a shoulder peak (α_3), respectively.⁴⁸⁻⁵⁰ The reduction of surface oxygen species for N- Co_3O_4 shifts to lower temperature compared with the M- Co_3O_4 (inset in Fig. 7). It implies that the oxygen species diffusion and activity in N- Co_3O_4 is accelerated significantly, which is in accordance with its higher catalytic activity.^{48,51} Compared with the reported traditional nanocasted Co_3O_4 replicas, three reduction peaks for both Co_3O_4 samples synthesized in this work shift a lot towards lower temperatures (for example, α_2 peak corresponding to the reduction of Co_3O_4 to CoO, shifts from 300-335 °C to 280 °C),⁴²⁻⁴⁴ revealing the calcination systems induced nanocasting method promote the reducibility and oxygen mobility of Co_3O_4 and enhance the CO oxidation activity.⁵² As we know, for the CO oxidation on Co_3O_4 catalytic material, CO firstly preferably adsorbed on the Co^{3+} , and then reacted with the lattice oxygen to produce CO_2 and oxygen vacancy. Then O_2 would react with the oxygen vacancy to reproduce the new active oxygen species and complete the whole redox cycle.⁴⁸ Hence, the surface oxygen species and the Co^{3+} concentration play important roles in the CO oxidation reaction. In Fig. 7, the ratio of the peak area α_2 to α_3 for N- Co_3O_4 is larger than that of M- Co_3O_4 corresponding to the higher Co^{3+}/Co^{2+} ratio in N- Co_3O_4 , which has been reported that abundant Co^{3+} ions possibly increase the anionic defect position and lead to higher catalytic activity for CO oxidation.^{53,54}

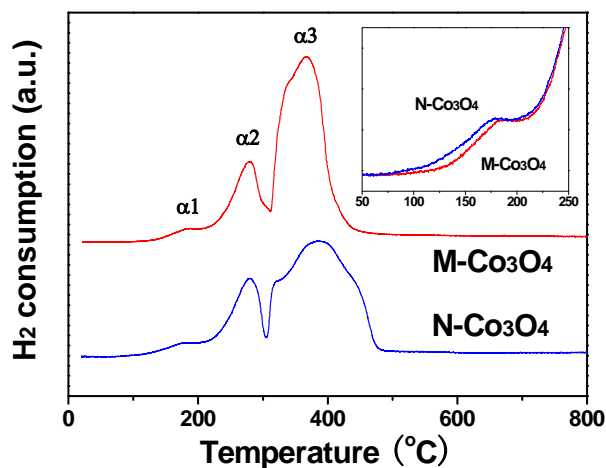
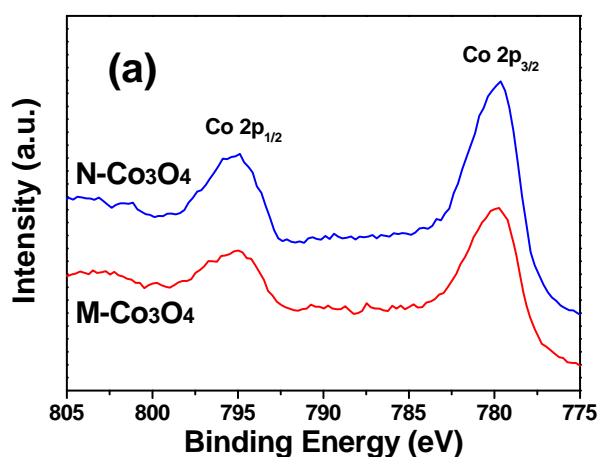


Fig. 7 H₂-TPR profiles of M-Co₃O₄ and N-Co₃O₄.

To illuminate the surface composition and valence state of the elements existing in Co₃O₄ samples, XPS spectra was performed as shown in Fig. 8. The elemental binding energies of these elements were corrected based on Carbon (C) 1S binding energy at 284.5 eV. Fig. 8a shows the XPS results of Co 2p of M-Co₃O₄ and N-Co₃O₄ samples. According to the literatures, it is hard to distinguish Co²⁺ from Co³⁺ by their BE values in Co 2p spectra.⁵⁵ However, the oxidation state of Co can be distinguished by the spin-orbit splitting of Co 2p peaks (ΔE). The ΔE value was reported to be 16.0 eV for CoO, 15.0 eV for Co₂O₃, and 15.2 eV for mixed valence Co₃O₄.⁵⁶ In this work, the ΔE values for both M-Co₃O₄ and N-Co₃O₄ are 15.25 eV, which can be seen clearly that Co₃O₄ is the main phase on the surface for both Co₃O₄ catalysts. Fig. 8b shows experimental and fitting XPS spectra of O1s for both Co₃O₄ samples. According to the references, the O 1s peaks were curve-fitted with three kinds of Gaussian peaks.^{57,58} The O 1s peaks of the binding energy for M-Co₃O₄ are observed at 529.5, 531.6 and 533.4 eV, respectively, corresponding to the surface lattice oxygen (O_{latt}, O²⁻),

surface absorbed oxygen (O_{ads} , e.g., O_2^- , O_2^{2-} or O^-), and the surface adsorbed water species.^{13,59} The fitting O 1s peaks for N-Co₃O₄ at 529.7, 531.6 and 533.5 eV can also be assigned to the surface lattice oxygen (O_{latt}), absorbed oxygen (O_{ads}), and adsorbed molecular water. The atomic ratio percentage of surface absorbed oxygen for M-Co₃O₄ (48.48%) is calculated to be larger than that of N-Co₃O₄ (28.23%), which is not consistent with the H₂-TPR and CO oxidation results. It indicates that the catalytic activities of Co₃O₄ samples synthesized in this work are not simply determined by adsorbed oxygen amount, which was also observed by He et al.⁵⁷ Because XPS can only quantify elements on the materials' surface, the pore structure and larger specific surface area of the as-synthesized Co₃O₄ in this work do not have an edge.⁴⁴ Combined with the H₂-TPR and N₂ physisorption results, the enhanced CO oxidation catalytic performance of N-Co₃O₄ comes from the high surface area and large porous size distribution, which is beneficial for the diffusion and adsorption of surface oxygen and the surface catalytic reaction.



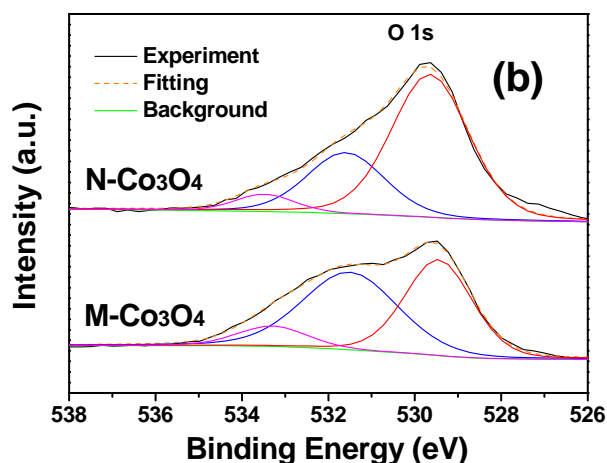


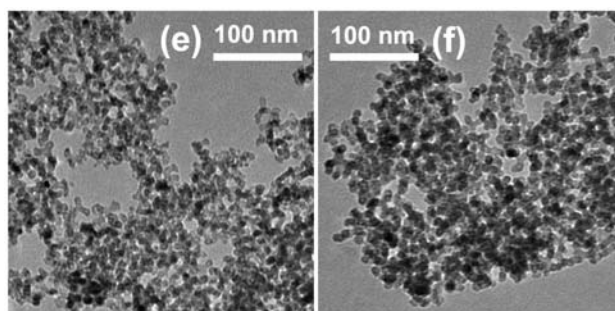
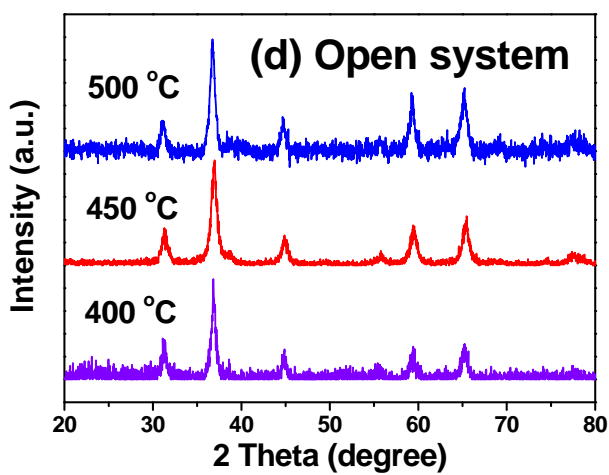
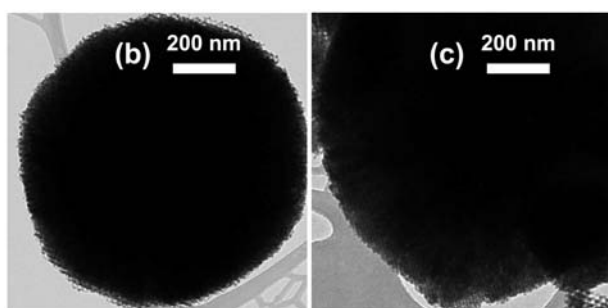
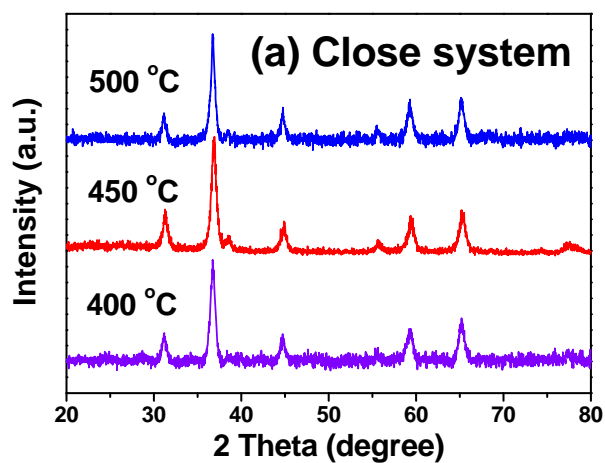
Fig. 8 Co 2p (a) and O 1s (b) XPS spectra of M-Co₃O₄ and N-Co₃O₄.

The above CO oxidation data show that N-Co₃O₄ replicas exhibit better catalytic properties than M-Co₃O₄ samples, suggesting the calcination system induced nanocasting synthesis methods have an important influence on Co₃O₄ activity. Changing of the calcination systems for nanocasting of Co₃O₄ demonstrated an obvious effect on the morphology and structure of catalysts. When using open system for the nanocasting calcination, N-Co₃O₄ replicas would be achieved in compared with M-Co₃O₄ obtained due to the close system nanocasting synthesis. According to the XRD, SAXRD, SEM, TEM, N₂ physisorption, and H₂-TPR results, we can see that N-Co₃O₄ had a much more uniform nanostructure with higher specific surface areas and larger porous size distribution than that of M-Co₃O₄, which exhibited highly ordered mesoporous structure with larger particle size and long-range mesoporous periodicity. Based on the transport phenomena and surface chemistry research for catalytic reaction, the improvement of diffusion and adsorption of reactant molecules are suggested to be the major factors for promoting the catalytic performance.¹¹ N-Co₃O₄ samples are with uniform nanoscale particle size (see Fig. 2), large pore size distribution (see Fig. 3, from ca. 6.0 nm to ca. 39 nm), and high specific surface area of 130.2 m² g⁻¹, corresponding to expose more clean surface active sites⁴⁴ and Co³⁺ cationic species (see Fig. 1 and Fig. 7). These

special structures of N-Co₃O₄ are favorable for the more effective surface adsorption and transfer of reactant molecules oxygen and CO and the catalytic products, and then improve the activity reaction of N-Co₃O₄ for CO oxidation.

In this work, the calcination temperatures effects on the structure, morphology and catalytic properties of the as-synthesized Co₃O₄ using nanocasting method with different calcination container systems have also been researched in detail. The XRD patterns of the as-synthesized Co₃O₄ in close system at different calcination temperatures are shown in Fig. 9a. From the XRD data, one can see that all of the diffraction peaks of Co₃O₄ synthesized at different temperatures correspond well to the face-centered cubic spinel phase of Co₃O₄ (JCPDS card No. 42-1467).^{25,41} With the increase of the calcination temperature, there is a little increase in the crystallite size, corresponding to the tiny heightening of each XRD pattern peak. The mesoporous morphology (TEM images shown in Fig. 9b, c and Fig. 2a) of the as-synthesized Co₃O₄ in close system at different calcination temperatures are almost the same with the similar wide particle size distribution and long-range mesoporous periodicity. The XRD patterns and TEM images of Co₃O₄ synthesized in open system at different calcination temperatures are shown in Fig. 9d, e, f and Fig. 2b, which indicated that calcination temperatures do not affect the crystallinity and nanoscale morphology of the as-synthesized Co₃O₄ in open system too much. From the above contrast data, one can see that calcination temperature is not a crucial factor to affect the mesoporous or nanoscale morphology of Co₃O₄ synthesized using nanocasting method, which was also observed on the nanocasting synthesis of Fe₂O₃ previously reported in our another work³⁸. Hence, it is found that the crystallinity and morphology are mainly determined by the calcination container

system and not by the calcination temperature. This is because the decomposition of metal nitrate precursors such as $\text{Co}(\text{NO}_3)_2$ or $\text{Fe}(\text{NO}_3)_3$ is at 100-200 °C.³⁸ For close system synthesis, fast water evaporation is prevented during the calcination, which keeps the precursor decomposition in a liquid form and obtains the long-range ordered mesoporous morphology at low temperature. In open system, before the decomposition of metal nitrate, the precursors turn to solid form and the solid-to-solid conversion happens and inhibits the long-distance transportation of the metal species and thus isolated nanoscale particles are formed. Hence, further high temperature calcination will not change the morphology of the as-synthesized Co_3O_4 any more. The catalytic contrast properties test shown in Fig. 9g and Fig. 5a indicated that the as-synthesized Co_3O_4 at the same calcination container system with different calcination temperature are also with similar catalytic performance, which corresponds to their similar structure and morphology.



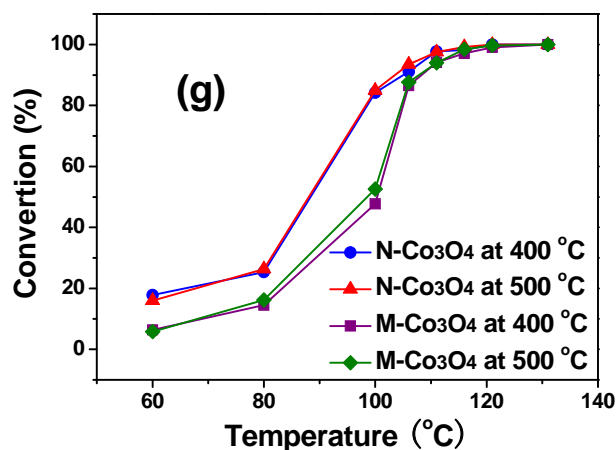


Fig. 9 XRD patterns (a) of Co_3O_4 synthesized in close system at different calcination temperatures (400, 450 and 500 °C); TEM images of Co_3O_4 synthesized in close system at 400 °C (b) and 500 °C (c); XRD patterns (d) of Co_3O_4 synthesized in open system at different calcination temperatures (400, 450 and 500 °C); TEM images of Co_3O_4 synthesized in open system at 400 °C (e) and 500 °C (f); conversion (g) as a function of temperature for CO oxidation over Co_3O_4 synthesized at different calcination temperatures and container systems.

Conclusions

Calcination system-induced nanocasting synthesis was used to prepare Co_3O_4 with controlled morphology and structure. Mesoporous M- Co_3O_4 synthesized at close calcination system have long-range mesoporous periodicity, large particle size, and high crystallinity. In contrast, nanoscale N- Co_3O_4 obtained at open calcination system exhibit uniform nanoparticle morphology with high specific surface area and large pore size distribution. Concerning the CO oxidation, the N- Co_3O_4 catalysts show enhanced CO conversion activity ($T_{50} = 88$ °C, $T_{100} = 121$ °C) in comparison with M- Co_3O_4 ($T_{50} = 100$ °C, $T_{100} = 131$ °C). N- Co_3O_4 with uniform nanoparticle morphology (ca. 10 nm) and high specific surface area ($130.2 \text{ m}^2 \text{ g}^{-1}$) increased the amount of surface clean active sites, and enhanced the adsorption of CO and activation of O_2 . The reactant diffusion and reducibility of N- Co_3O_4 were significantly

promoted due to the presence of large pore size distribution and enough surface adsorbed oxygen species. Therefore, the enhanced CO oxidation performance of N-Co₃O₄ is attributed to its uniform nanostructure, high specific surface area, large porous distribution, and abundant active sites. This improved nanocasting approach may be applicable to the synthesis of other metal oxides materials with uniform nanostructure and high catalytic activity.

Acknowledgements

This work was supported by funding from the National Natural Science Foundation of China, NSFC (51202159, 51208357, 51472179), Fund for the Doctoral Program of Higher Education, Ministry of Education of China (20120032120017), General Program of Municipal Natural Science Foundation of Tianjin (13JCYBJC16900, 13JCQNJC08200).

Notes and references

- 1 Q. Zhang, H. Y. Wang, X. Jia, B. Liu and Y. Yang, One-dimensional metal oxide nanostructures for heterogeneous catalysis, *Nanoscale*, 2013, **5**, 7175-7183.
- 2 Z. X. Li, W. Xue, B. T. Guan, F. B. Shi, Z. J. Shi, H. Jiang and C. H. Yan, A conceptual translation of homogeneous catalysis into heterogeneous catalysis: homogeneous-like heterogeneous gold nanoparticle catalyst induced by ceria supporter, *Nanoscale*, 2013, **5**, 1213-1220.
- 3 A. F. Lee, J. A. Bennett, J. C. Manayil and K. Wilson, Heterogeneous catalysis for sustainable biodiesel production via esterification and transesterification, *Chem. Soc. Rev.*, 2014, **43**, 7887-7916.
- 4 Z. Guo, B. Liu, Q. Zhang, W. Deng, Y. Wang and Y. Yang, Recent advances in heterogeneous selective oxidation catalysis for sustainable chemistry, *Chem. Soc. Rev.*, 2014, **43**, 3480-3524.
- 5 J. K. Norskov, T. Bligaard, B. Hvolbaek, F. Abild-Pedersen, I. Chorkendorff and C. H. Christensen, The nature of the active site in heterogeneous metal catalysis, *Chem. Soc. Rev.*, 2008, **37**, 2163-2171.
- 6 K. Q. Sun, Y. C. Hong, G. R. Zhang and B. Q. Xu, Synergy between Pt and Au in Pt-on-Au nanostructures for chemoselective hydrogenation catalysis, *ACS Catal.*, 2011, **1**, 1336-1346.
- 7 T. Blasco, Insights into reaction mechanisms in heterogeneous catalysis revealed by in situ NMR spectroscopy, *Chem. Soc. Rev.*, 2010, **39**, 4685-4702.
- 8 A. M. H. Rasmussen, M. N. Groves and B. Hammer, Remote activation of chemical bonds in heterogeneous catalysis, *ACS Catal.*, 2014, **4**, 1182-1188.
- 9 D. Astruc, F. Lu and J. R. Aranzas, Nanoparticles as recyclable catalysts: The frontier between homogeneous and heterogeneous catalysis, *Angew. Chem.-Int. Edit.*, 2005, **44**, 7852-7872.
- 10 Y. Bai, W. H. Zhang, Z. H. Zhang, J. Zhou, X. J. Wang, C. M. Wang, W. X. Huang, J. Jiang and Y. J. Xiong, Controllably interfacing with metal: A strategy for enhancing CO oxidation on oxide catalysts by surface polarization, *J. Am. Chem. Soc.* 2014, **136**, 14650-14653.

- 11 H. Kuhlenbeck, S. Shaikhutdinov and H.J. Freund, Well-ordered transition metal oxide layers in model catalysis - A series of case studies, *Chem. Rev.*, 2013, **113**, 3986-4034.
- 12 B. K. Min and C. M. Friend, Heterogeneous gold-based catalysis for green chemistry: Low-temperature CO oxidation and propene oxidation, *Chem. Rev.*, 2007, **107**, 2709-2724.
- 13 S. Xie, H. Dai, J. Deng, Y. Liu, H. Yang, Y. Jiang, W. Tan, A. Ao and G. Guo, Au/3DOM Co₃O₄: highly active nanocatalysts for the oxidation of carbon monoxide and toluene, *Nanoscale*, 2013, **5**, 11207-11219.
- 14 Z. Ma, B. Zhou and Y. Ren, Crystalline mesoporous transition metal oxides: hard-templating synthesis and application in environmental catalysis, *Front. Env. Sci. Eng.*, 2013, **7**, 341-355.
- 15 S. Royer and D. Duprez, Catalytic oxidation of carbon monoxide over transition metal oxides, *Chemcatchem*, 2011, **3**, 24-65.
- 16 P. Chen, J. Q. Lu, G. Q. Xie, G. S. Hu, L. Zhu, L. F. Luo, W. X. Huang and M. F. Luo, Effect of reduction temperature on selective hydrogenation of crotonaldehyde over Ir/TiO₂ catalysts, *Appl. Catal. A-Gen.*, 2012, **433**, 236-242.
- 17 K. B. Zhou, X. Wang, X. M. Sun, Q. Peng and Y. D. Li, Enhanced catalytic activity of ceria nanorods from well-defined reactive crystal planes, *J. Catal.*, 2005, **229**, 206-212.
- 18 S. Schauermaun, N. Nilius, S. Shaikhutdinov and H. J. Freund, Nanoparticles for heterogeneous catalysis: new mechanistic insights, *Accounts Chem. Res.*, 2013, **46**, 1673-1681.
- 19 J. Zhu, T. Wang, X. Xu, P. Xiao and J. Li, Pt nanoparticles supported on SBA-15: Synthesis, characterization and applications in heterogeneous catalysis, *Appl. Catal. B-Environ.*, 2013, **130**, 197-217.
- 20 A. Arango-Diaz, E. Moretti, A. Talon, L. Storaro, M. Lenarda, P. Nunez, J. Marrero-Jerez, J. Jimenez-Jimenez, A. Jimenez-Lopez and E. Rodriguez-Castellon, Preferential CO oxidation (CO-PROX) catalyzed by CuO supported on nanocrystalline CeO₂ prepared by a freeze-drying method, *Appl. Catal. A-Gen.*, 2014, **477**, 54-63.
- 21 L. Lietti, I. Nova and P. Forzatti, Role of ammonia in the reduction by hydrogen of NO_x stored over Pt-Ba/Al₂O₃ lean NO_x trap catalysts, *J. Catal.*, 2008, **257**, 270-282.
- 22 M. M. Natile and A. Glisenti, New NiO/Co₃O₄ and Fe₂O₃/Co₃O₄ nanocomposite catalysts: Synthesis and characterization, *Chem. Mater.*, 2003, **15**, 2502-2510.
- 23 I. E. Wachs and C. A. Roberts, Monitoring surface metal oxide catalytic active sites with Raman spectroscopy, *Chem. Soc. Rev.*, 2010, **39**, 5002-5017.
- 24 F. J. Liu, S. F. Zuo, X. D. Xia, J. Sun, Y. C. Zou, L. Wang, C. G. Li and C. Z. Qi, Generalized and high temperature synthesis of a series of crystalline mesoporous metal oxides based nanocomposites with enhanced catalytic activities for benzene combustion, *J. Mater. Chem. A*, 2013, **1**, 4089-4096.
- 25 N. Yan, Q. Chen, F. Wang, Y. Wang, H. Zhong and L. Hua, High catalytic activity for CO oxidation of Co₃O₄ nanoparticles in SiO₂ nanocapsules, *J. Mater. Chem. A*, 2013, **1**, 637-643.
- 26 Y. Li, Q. Y. Liu, W and J. Shen, Morphology-dependent nanocatalysis: metal particles, *Dalton Trans.*, 2011, **40**, 5811-5826.
- 27 S. T. Marshall, M. O'Brien, B. Oetter, A. Corpuz, R. M. Richards, D. K. Schwartz and J. W. Medlin, Controlled selectivity for palladium catalysts using self-assembled monolayers, *Nat. Mater.*, 2010, **9**, 853-858.
- 28 R. Narayanan and M. A. El-Sayed, Effect of catalysis on the stability of metallic nanoparticles: Suzuki reaction catalyzed by PVP-palladium nanoparticles, *J. Am. Chem. Soc.*, 2003, **125**, 8340-8347.
- 29 Y. Q. Wang, C. M. Yang, W. Schmidt, B. Spliethoff, E. Bill and F. Schuth, Weakly ferromagnetic ordered mesoporous Co₃O₄ synthesized by nanocasting from vinyl-functionalized cubic Ia3d mesoporous silica, *Adv. Mater.*, 2005, **17**, 53.

- 30 G. Li, D. Zhang and J. C. Yu, Ordered mesoporous BiVO₄ through nanocasting: A superior visible light-driven photocatalyst, *Chem. Mater.*, 2008, **20**, 3983-3992.
- 31 S. Polarz and M. Antonietti, Porous materials via nanocasting procedures: innovative materials and learning about soft-matter organization, *Chem. Commun.*, 2002, 2593-2604.
- 32 H. F. Yang and D. Y. Zhao, Synthesis of replica mesostructures by the nanocasting strategy, *J. Mater. Chem.*, 2005, **15**, 1217-1231.
- 33 A. H. Lu and F. Schuth, Nanocasting: A versatile strategy for creating nanostructured porous materials, *Adv. Mater.*, 2006, **18**, 1793-1805.
- 34 X. Sun, H. Hao, H. Ji, X. Li, S. Cai and C. Zheng, Nanocasting synthesis of In₂O₃ with appropriate mesostructured ordering and enhanced gas-sensing property, *ACS Appl. Mater. Interfaces*, 2014, **6**, 401-409.
- 35 F. Jiao, A. Harrison, J. C. Jumas, A. V. Chadwick, W. Kockelmann and P. G. Bruce, Ordered mesoporous Fe₂O₃ with crystalline walls, *J. Am. Chem. Soc.*, 2006, **128**, 5468-5474.
- 36 B. Z. Tian, X. Y. Liu, H. F. Yang, S. H. Xie, C. Z. Yu, B. Tu and D. Y. Zhao, General synthesis of ordered crystallized metal oxide nanoarrays replicated by microwave-digested mesoporous silica, *Adv. Mater.*, 2003, **15**, 1370.
- 37 A. Ruplecker, F. Kleitz, E. L. Salabas and F. Schueth, Hard templating pathways for the synthesis of nanostructured porous Co₃O₄, *Chem. Mater.*, 2007, **19**, 485-496.
- 38 X. Sun, Y. Shi, P. Zhang, C. Zheng, X. Zheng, F. Zhang, Y. Zhang, N. Guan, D. Zhao and G. D. Stucky, Container effect in nanocasting synthesis of mesoporous metal oxides, *J. Am. Chem. Soc.*, 2011, **133**, 14542-14545.
- 39 F. Kleitz, S. H. Choi and R. Ryoo, Cubic Ia3d large mesoporous silica: synthesis and replication to platinum nanowires, carbon nanorods and carbon nanotubes, *Chem. Commun.*, 2003, **17**, 2136-2137.
- 40 Y. H. Zu, P. P. Yang, J. J. Wang, X. H. Liu, J. W. Ren, G. Z. Lu and Y. Q. Wang, Efficient production of the liquid fuel 2,5-dimethylfuran from 5-hydroxymethylfurfural over Ru/Co₃O₄ catalyst, *Appl. Catal. B-Environ.*, 2014, **146**, 244-248.
- 41 X. Liu, Q. Long, C. Jiang, B. Zhan, C. Li, S. Liu, Q. Zhao, W. Huang and X. Dong, Facile and green synthesis of mesoporous Co₃O₄ nanocubes and their applications for supercapacitors, *Nanoscale*, 2013, **5**, 6525-6529.
- 42 S. Varghese, M.G. Cutrufello, E. Rombi, C. Cannas, R. Monaci and I. Ferino, CO oxidation and preferential oxidation of CO in the presence of hydrogen over SBA-15-templated CuO-Co₃O₄ catalysts, *Appl. Catal. A-Gen.*, 2012, **443**, 161-170.
- 43 Y. Wang, C. Zhang, F. Liu and H. He, Well-dispersed palladium supported on ordered mesoporous Co₃O₄ for catalytic oxidation of o-xylene, *Applied Catalysis B-Environmental*, 2013, **142**, 72-79.
- 44 B. Bai, H. Arandiyani, J. Li, Comparison of the performance for oxidation of formaldehyde on nano-Co₃O₄, 2D-Co₃O₄, and 3D-Co₃O₄ catalysts, *Appl. Catal. B-Environ.*, 2013, **142**, 677-683.
- 45 Y. Ren, Z. Ma, L. Qian, S. Dai, H. He and P. G. Bruce, Ordered crystalline mesoporous oxides as catalysts for CO oxidation, *Catal. Lett.*, 2009, **131**, 146-154.
- 46 I. Lopes, A. Davidson and C. Thomas, Calibrated Co₃O₄ nanoparticles patterned in SBA-15 silicas: Accessibility and activity for CO oxidation, *Catal. Commun.*, 2007, **8**, 2105-2109.
- 47 C. J. Jia, M. Schwickardi, C. Weidenthaler, W. Schmidt, S. Korhonen, B.M. Weckhuysen and F. Schueth, Co₃O₄-SiO₂ nanocomposite: A very active catalyst for CO oxidation with unusual catalytic behavior, *J. Am. Chem. Soc.*, 2011, **133**, 11279-11288.
- 48 Y. Lou, L. Wang, Z. Y. Zhao, Y. H. Zhang, Z. G. Zhang, G. Z. Lu, Y. Guo and Y. L. Guo,

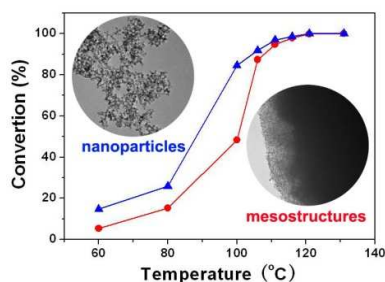
- Low-temperature CO oxidation over Co_3O_4 -based catalysts: Significant promoting effect of Bi_2O_3 on Co_3O_4 catalyst, *Appl. Catal. B-Environ.* 2014, **146**, 43-49.
- 49 L. Xue, C. B. Zhang, H. He and Y. Teraoka, Catalytic decomposition of N_2O over CeO_2 promoted Co_3O_4 spinel catalyst, *Appl. Catal. B-Environ.*, 2007, **75**, 167-174.
- 50 N. Bahlawane, E. F. Rivera, K. Kohse-Hoinghaus, A. Brechling and U. Kleineberg, Characterization and tests of planar Co_3O_4 model catalysts prepared by chemical vapor deposition, *Appl. Catal. B-Environ.*, 2004, **53**, 245-255.
- 51 L. Hu, Q. Peng and Y. Li, Selective synthesis of Co_3O_4 nanocrystal with different shape and crystal plane effect on catalytic property for methane combustion, *J. Am. Chem. Soc.*, 2008, **130**, 16136.
- 52 C. Y. Ma, Z. Mu, J. J. Li, Y. G. Jin, J. Cheng, G. Q. Lu, Z. P. Hao and S. Z. Qiao, Mesoporous Co_3O_4 and $\text{Au}/\text{Co}_3\text{O}_4$ catalysts for low-temperature oxidation of trace ethylene, *J. Am. Chem. Soc.*, 2010, **132**, 2608-2613.
- 53 M. Kang, M. W. Song and C. H. Lee, Catalytic carbon monoxide oxidation over CoOx/CeO_2 composite catalysts, *Appl. Catal. A-Gen.*, 2003, **251**, 143-156.
- 54 X. Xie, Y. Li, Z. Q. Liu, M. Haruta and W. Shen, Low-temperature oxidation of CO catalysed by Co_3O_4 nanorods, *Nature*, 2009, **458**, 746-749.
- 55 Y. Liu, B. Liu, Q. Wang, C. Li, W. Hu, Y. Liu, P. Jing, W. Zhao and J. Zhang, Three-dimensionally ordered macroporous $\text{Au}/\text{CeO}_2\text{-Co}_3\text{O}_4$ catalysts with mesoporous walls for enhanced CO preferential oxidation in H_2 -rich gases, *J. Catal.*, 2012, **296**, 65-76.
- 56 J. Y. Luo, M. Meng, X. Li, X. G. Li, Y. Q. Zha, T. D. Hu, Y. N. Xie and J. Zhang, Mesoporous $\text{Co}_3\text{O}_4\text{-CeO}_2$ and $\text{Pd}/\text{Co}_3\text{O}_4\text{-CeO}_2$ catalysts: Synthesis, characterization and mechanistic study of their catalytic properties for low-temperature CO oxidation, *J. Catal.*, 2008, **254**, 310-324.
- 57 Y. Wen, C. Zhang, H. He, Y. Yu and Y. Teraoka, Catalytic oxidation of nitrogen monoxide over $\text{La}_{1-x}\text{Ce}_x\text{CoO}_3$ perovskites, *Catal. Today*, 2007, **126**, 400-405.
- 58 A. Machocki, T. Ioannides, B. Stasinska, W. Gac, G. Avgouropoulos, D. Delimaris, W. Grzegorzczak and S. Pasieczna, Manganese-lanthanum oxides modified with silver for the catalytic combustion of methane, *J. Catal.*, 2004, **227**, 282-296.
- 59 J. Xu, J. Liu, Z. Zhao, C. Xu, J. Zheng, A. Duan and G. Jiang, Easy synthesis of three-dimensionally ordered macroporous $\text{La}_{1-x}\text{K}_x\text{CoO}_3$ catalysts and their high activities for the catalytic combustion of soot, *J. Catal.*, 2011, **282**, 1-12.

Calcination system-induced nanocasting synthesis of uniform Co_3O_4 nanoparticles with high surface area and enhanced catalytic performance

Xiaohong Sun,^{*,†} Rui You,[‡] Xudong Hu,[†] Junbin Mo,[†] Rui Xiong,[†] Huiming Ji,[†] Xiaolei Li,[†] Shu Cai,[†] Chunming Zheng^{*,§} and Ming Meng[‡]

Table of contents entry:

Nanoscale Co_3O_4 synthesized by open-system nanocasting with uniform size, high surface area, large pore-distribution and abundant active-sites exhibit improved catalysis.



[†]School of Materials Science and Engineering, Key Lab of Advanced Ceramics and Machining Technology, Tianjin University, Tianjin 300072, PR China. E-mail: sunxh@tju.edu.cn

[‡]School of Chemical Engineering and Technology, Tianjin University, Tianjin 300072, PR China.

[§]State Key Laboratory of Hollow-fiber Membrane Materials and Membrane Processes, School of Environmental and Chemical Engineering, Tianjin Polytechnic University, Tianjin 300387, PR China. E-mail: zhengchunming@tjpu.edu.cn